ACS OMEGA

Open Access

http://pubs.acs.org/journal/acsodf

Article

Photocatalytic Estrogen Degradation by the Composite of Tin Oxide Fine Particles and Graphene-like Carbon Nitride

Yuzuki Amino, Ayar Al-zubaidi, Yosuke Ishii, and Shinji Kawasaki*

Cite This: *ACS Omega* 2024, 9, 49064−49070

Read Online

ACCESS | Metrics & More | Article Recommendations | Supporting Information

ABSTRACT: This study investigates whether 17β-estradiol (E2), a natural estrogen and one of the endocrine-disrupting chemicals responsible for water pollution, can be oxidatively decomposed under simulated solar light using a composite of tin oxide nanoparticles and graphene-like carbon nitride (g-CN) as a photocatalyst. The composite photocatalyst was prepared by heating a mixture of urea and tin acetate. FT-IR measurements revealed that g-CN possesses structural units similar to g-C_3N_4, a well-studied graphite-like carbon nitride. However, unlike g-C_3N_4, sharp diffraction lines were not observed in the XRD diffraction pattern of g-CN, indicating lower crystallinity. Elemental analysis showed that g-CN is slightly nitrogen-rich compared to g-C_3N_4, and UV−vis measurements indicated that the band gap of g-CN is slightly smaller than that of g-C_3N_4. The presence of tin in the composite of tin oxide and g-CN was clearly confirmed by XPS, although no sharp diffraction peaks were observed in the XRD patterns, suggesting the presence of microcrystals. Furthermore, FE-SEM observations did not reveal large tin oxide crystals, although EDS mapping indicated the presence of tin oxide. It was found that the prepared tin oxide and g-CN composites function effectively as photocatalysts for degrading E2 under simulated solar light. The degradation rate constant was evaluated to be k = 3.34 (0.14) × 10^{-2} min^{-1}. Peroxide ion radicals were detected in ESR measurements from the irradiated solution, suggesting that peroxide ion radicals are generated through oxygen photoreduction as the counter-reaction of the oxidative decomposition of E2.

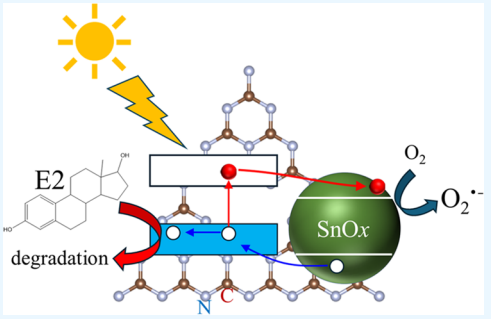

INTRODUCTION

The ecological impact of endocrine disruptors (environmental hormones) present in trace amounts in rivers has been a prominent concern.[1,2] Through numerous investigations, rivers have been revealed to be contaminated with natural estrogens such as estrone (E1), 17β-estradiol (E2), estriol (E3), and synthetic estrogens like ethinyl estradiol.[3,4] These compounds can cause harmful effects such as feminization, infertility, and hermaphroditism in organisms inhabiting water bodies. Therefore, there is a strong demand to remove these estrogens for environmental purification.

Since the 1990s, quantitative experiments have been conducted to evaluate the impact of the aforementioned estrogen on aquatic life, such as fish, in rivers.[5] Among the three types of estrogens mentioned, E2 is known to have a significant physiological effect.[5] It has been pointed out that as little as 10 ng/L of E2 can cause feminization in fish. In response to this, the removal of E2 in sewage treatment has become a critical issue, leading to active research into advanced oxidation processes, including the use of ozone, in addition to the general chlorine-based oxidizing agents for E2 degradation. Detailed studies on the oxidative decomposition process of E2 have also been conducted during this time, revealing the intermediate products through which the degradation progresses.

In recent years, there has been an active effort to use photocatalysts for environmental purification.[6,7] Using energy derived from fossil fuels for environmental purification can exacerbate environmental pollution during energy generation. By contrast, combining solar energy with photocatalysts for the purification process does not cause new environmental problems.

Among the various photocatalyst materials studied for this purpose, graphite-like carbon nitride (g-C_3N_4) has recently gained significant attention as a metal-free photocatalyst under visible light irradiation, as it is composed of only abundant elements, easy to synthesize, and chemically stable.[8−13] The basic tectonic units to establish g-C_3N_4 allotropes are considered to be triazine (C_3N_3) and tri-s-triazine/heptazine (C_6N_7) rings, although the samples actually synthesized may have several polymorphs with slightly different structures (Figure S1). The history of g-C_3N_4 dates back to 1834 when the embryonic form of melon was first developed.[14] After

Received: April 9, 2024
Revised: October 11, 2024
Accepted: October 16, 2024
Published: December 6, 2024

Wang reported its excellent photocatalytic hydrogen generation ability, g-C_3N_4 gained attention as a photocatalyst.[15] Subsequently, extensive research has been conducted on the photocatalytic applications of g-C_3N_4. Much of this research is driven by the perspective of addressing environmental issues.[16−18]

It has recently been reported that g-C_3N_4/SnO_2 composite can be a visible light photocatalyst capable of photocatalytic degradation of Rhodamine B.[19] Ji reported that Rhodamine B is oxidatively decomposed by the holes generated by the photoexcitation of electrons.[14] If the same mechanism can be applied to the photocatalytic degradation of environmental hormones, river purification and environmental purification can be ideally achieved. To demonstrate this, this study synthesized g-C_3N_4/SnO_2 composites and investigated their photocatalytic activity in decomposing E2 (Figure S2), which was used as the representative form of estrogen. This research aims to develop a photocatalyst that allows for the decomposition of estrogen by solar light. The specific purpose of this experiment is to verify whether a composite of tin oxide nanoparticles and graphene-like carbon nitride can effectively decompose E2 under the irradiation of solar light. Therefore, experiments were conducted using a high concentration (0.1 mM) aqueous solution of E2, compared to the actual concentration of E2 found in rivers (on the order of several ng/L).

EXPERIMENTAL SECTION

The g-C_3N_4/SnO_2 composites were synthesized through a previously reported procedure.[16] It should be noted although referred to as g-C_3N_4 in this paper, the g-C_3N_4 synthesized in the present study is somewhat structurally distorted, as will be discussed in the next section. To synthesize the composite, a mixture of urea (Nacalai Tesque Inc.) and tin(II) acetate (Sigma-Aldrich Co.) was placed in a crucible and thermally treated at 550 °C for 2 h under N_2 flow in an electric furnace to obtain the g-C_3N_4/SnO_2 composite. Various weight percentages of tin(II) acetate (0, 0.3, 0.6, and 1.5 wt %) were used to prepare the mixture. The corresponding composites were abbreviated as CNSnO-0, CNSnO-0.3, CNSnO-0.6, and CNSnO-1.5. The synthesized composite samples were characterized through spectroscopic experiments such as Fourier-transform infrared spectroscopy (FT-IR), X-ray diffraction (XRD), and X-ray photoelectron spectroscopy (XPS). FT-IR, XRD and XPS measurements were performed using FT/IR-6300 (JASCO Co.), Rigaku Miniflex (Rigaku Co.) and PHI Quantes (ULVAC-PHI Inc.). Elemental analysis of H, C, N was done on vario EL cube (Elementar) and the N/C ratio was also evaluated using XPS. For the FT-IR measurements, a pellet was made by mixing KBr powder with the sample and then measuring by the transmission method. The XPS measurements were conducted by pressing the sample powder onto In foil. FE-SEM (EDS) and TEM measurements were carried out using a JSM-7800F (JEOL) and a JEM-Z2500 (JEOL), respectively. UV−vis measurements were performed using Shimadzu UV-1900i spectrophotometer, and analysis based on the Kubelka−Munk theory was conducted to estimate the band gap of the carbon nitride composite samples.[17] The AC impedance measurements of the sample were performed using an Autolab PGSTAT128N, and the flat band potential was estimated from the Mott−Schottky plot. We also performed nitrogen adsorption/desorption isotherm measurements on the prepared samples at 77 K using a Gemini 2375 (Shimadzu). The Brunauer−Emmett−Teller (BET) surface area values of the samples were determined from the observed N_2 adsorption isotherms.

Estradiol (E2) was purchased from Nacalai Tesque Inc. A solution of 0.1 mM E2 with the CNSnO composite was stirred in the dark for 3 h to avoid causing any light-induced changes prior to the photoirradiation experiment. Subsequently, the solution was irradiated with simulated sunlight from a solar simulator (AM1.5G, 1000 W/m^2). After irradiation, the solution was centrifuged to remove the composite samples, and the change in E2 concentration was examined via photoluminescence (PL) measurements. PL measurements were carried out on FP-8600 (JASCO Co.). To investigate the mechanism of CNSnO-catalyzed E2 photodegradation, Electron spin resonance (ESR) measurements using 5,5-Dimethyl-4-phenyl-1-pyrroline N-Oxide (DMPO) purchased from Tokyo Chemical Industry Co. as a radical trapping agent were carried out to detect the reduced species in the degradation process. The ESR measurements were performed using a JES-FA200 (JEOL) at an observation frequency of 9.055 GHz.

RESULTS AND DISCUSSION

The FT-IR spectra of the prepared CNSnO-0 and CNSnO-0.3 are shown in Figure 1. In both samples, characteristic g-C_3N_4 peaks are observed, including the triazine breathing mode around 810 cm^{-1} (marked with asterisk) and peaks corresponding to C−N and C═N stretching vibrations in the range of 1100−1600 cm^{-1}.[20] Therefore, the synthesized samples can be inferred to possess the basic units of g-C_3N_4. However, XRD measurements of CNSnO-0 resulted in only a broad halo pattern (Figure S3), whereas highly crystalline g-C_3N_4 exhibits diffraction lines indicative of a layered structure of hexagonal network planes and regular structures within the plane (Figures S1 and S4).[21] Therefore, we hypothesize that the CNSnO composites synthesized in this study have a somewhat distorted network structure of triazine and/or tri-s-triazine units.

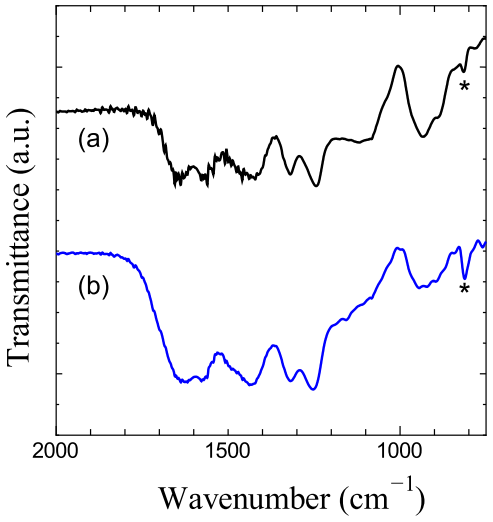

Figure 1. FT-IR spectra of (a) CNSnO-0 and (b) CNSnO-0.3.

Furthermore, XRD diffraction patterns of CNSnO-0.3 also show only broad diffraction lines, and no diffraction lines attributable to SnO_2 crystals are observed (Figure S3).

https://doi.org/10.1021/acsomega.4c03390
ACS Omega 2024, 9, 49064−49070

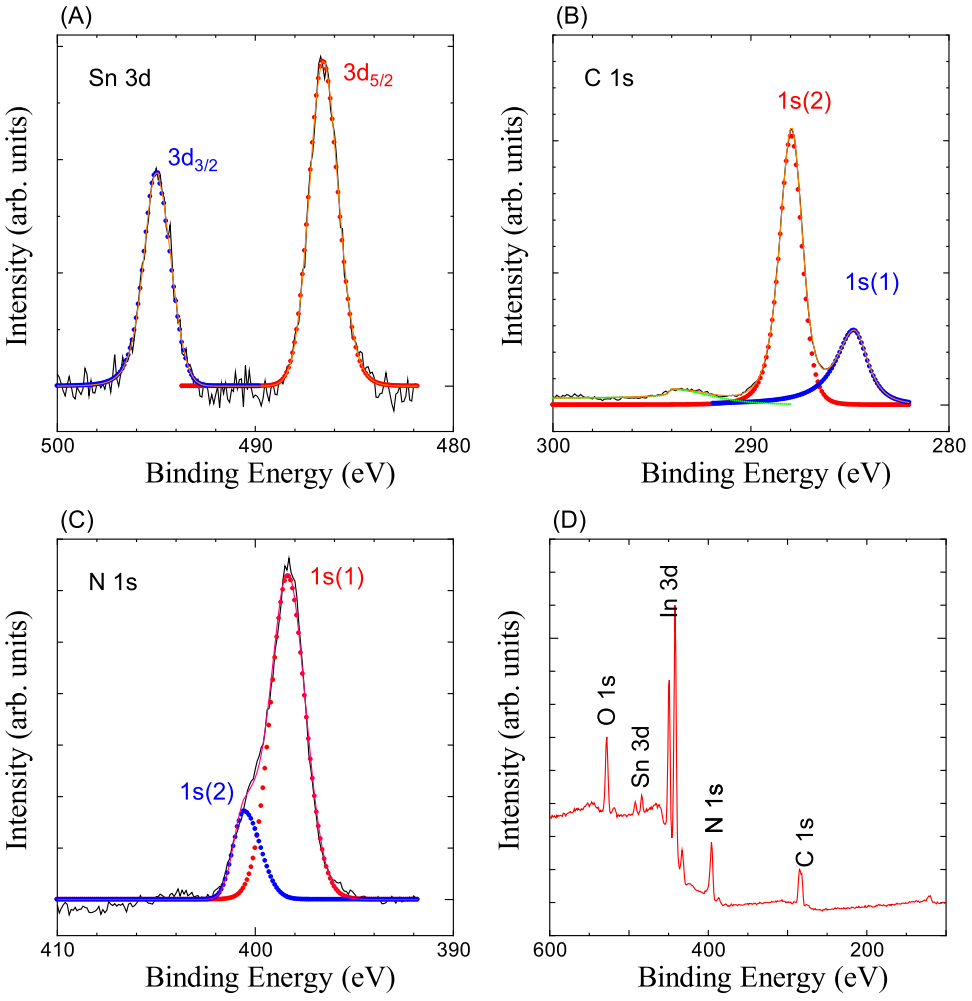

Figure 2. (A) Sn 3d, (B) C 1s, (C) N 1s, (D) wide XPS spectra of CNSnO-0.3.

However, XPS measurements confirm the clear presence of Sn (Figure 2A).[22] Therefore, it is plausible that CNSnO-0.3 contains amorphous Sn oxides or ultra fine Sn oxide crystals. Thermogravimetric (TG) measurements of CNSnO-0.3 in air revealed residual tin oxide of about 1.5 wt %. Additionally, elemental analysis revealed an N/C ratio of approximately 1.354, indicating a nitrogen-rich composition compared with g-C_3N_4.

As mentioned above, the Sn 3d peaks are clearly observed in the XPS spectrum of CNSnO-0.3 (Figure 2A), confirming the presence of Sn. Additionally, the peak energy positions (Sn $3d_{5/2}$ = 486.6, $3d_{3/2}$ = 495.0 eV) suggest that Sn is in the +4 oxidation state (Figure S5A, Table S1). However, the O 1s XPS spectrum shows a broad peak, indicating that the presence of Sn in lower oxidation states cannot be definitively ruled out (Figure S5C). The C 1s XPS spectrum of CNSnO-0.3 exhibits peaks around 284.7 and 288 eV (Figure 2B). The high-energy-side peak can be explained by C bonded with N and is consistent with the structure of g-C_3N_4 (Figure S1). However, the 284.7 eV peak cannot be explained by the g-C_3N_4 structure shown in Figure S1. This peak may be due to carbon clusters, the presence of sp^3 carbon, or contaminant carbon. Changing the measurement location revealed variations in the intensity of this peak, suggesting that it is caused by some type of impurity (Figure S5B). This low-energy-side C 1s peak is often reported in studies describing the synthesis of g-C_3N_4.

The strong peak around 398.5 eV in the N 1s spectrum (Figure 2C) is attributed to nitrogen in the triazine structure of the g-C_3N_4 structural unit. The high-energy-side shoulder peak (around 400.6 eV) is attributed to nitrogen in the C−N═N−C structure, as observed in g-C_3N_5.[23] Taking these findings into consideration, we conclude that the synthesized CNSnO composite shares many structural similarities with g-C_3N_4 shown in Figure S1, but is slightly nitrogen-rich and lacks crystalline integrity (Figure 2D).

In the FE-SEM image of the CNSnO-0.3 sample (Figure S6B), sheet-like carbon nitride can be observed, but distinct crystals of tin oxide are not visible. However, as previously mentioned, tin was detected by XPS, and tin was also detected in the SEM-attached EDS (Figure S8). The specific location of Sn is difficult to determine through EDS mapping, suggesting that tin oxide is homogeneously deposited throughout the sample. TEM observations showed a sheet-like structure of CNSnO-0.3, with what appear to be Sn oxide nanoparticles dispersed on the sheet surface (Figure S7). The BET specific surface area of the CNSnO-0.3 sample, determined by N_2 gas adsorption measurements, is 68.0 cm^2/g (Table S2), which is relatively large for g-C_3N_4-related samples. This relatively large specific surface area can be attributed to the inhibition of graphene-like sheet stacking due to the simultaneous synthesis with tin oxide. This is consistent with the absence of sharp

https://doi.org/10.1021/acsomega.4c03390
ACS Omega 2024, 9, 49064−49070

diffraction peaks related to sheet stacking in the XRD patterns (Figure S3).

Next, we discuss the photodegradation performance of the CNSnO composite. Figure 3 shows the extent of decrease in the PL peak intensity around 305 nm of E2 after 1 h of photoirradiation of the solutions including CNSnO-0 and CNSnO-0.3 composites.[24] As shown in the figure, the photoirradiation of CNSnO-0 causes no significant change in the E2 peak shape, albeit for a light decrease in the peak's PL intensity, suggesting that E2 degradation has hardly occurred. By contrast, the photoirradiation of CNSnO-0.3 caused the peak intensity around 305 nm to decrease significantly after 1 h of photoirradiation, and a new broad peak appeared on the high-wavelength side. This indicates that upon using CNSnO-0.3, E2 is decomposed by light irradiation, leading to a decrease in the peak intensity around 305 nm and the formation of new broad peaks on the high-wavelength side due to the generation of decomposition products. In other words, the carbon nitride CNSnO-0, which is structurally similar to g-C_3N_4, does not cause E2 photodegradation on its own. By contrast, E2 degradation becomes possible on carbon nitride with the addition of Sn oxides. Although the amount of Sn oxide has not been optimized, we predict that the performance is sufficient at a level close to that of CNSnO-0.3, because using CNSnO-0.6 that includes twice the amount of Sn did not significantly improve the performance. For these reasons, this paper will focus on the data for CNSnO-0.3 in the main text.

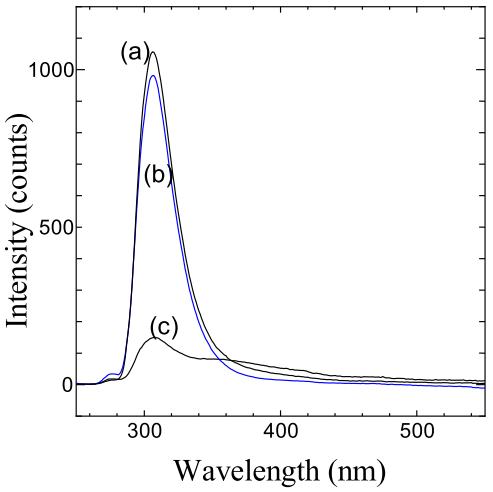

Figure 3. PL intensity of E2 (a) before photoirradiation, and after photoirradiation for 1 h with (b) CNSnO-0 and (c) CNSnO-0.3.

In this study, we did not analyze the photodegradation process of E2 when using CNSnO-0.3 as the photocatalyst. However, based on previous reports, it is believed that the degradation proceeds via the intermediate 10ε-17β-dihydroxy-1,4-estradien-3-one (DEO) (Figure S2).[25,26] As the degradation progresses, the biological impact of E2 is, of course, eliminated. Additionally, it has been reported that the interaction of DEO, the intermediate product, with estrogen receptors is significantly reduced compared to E2.[25,26]

Next, we discuss the changes in E2 photodegradation by CNSnO-0.3 with the duration of light irradiation. As shown in Figure 4A, it is evident that the PL intensity of E2 decreases with increasing the irradiation time. The plot in the figure represents the integrated intensity of the peak around 305 nm as a function of the irradiation time.

As observed in Figure 4B, the peak intensity exhibits an exponential decrease with respect to the irradiation time (Figure S9). Considering that the peak intensity is proportional to the concentration of E2, we calculated the first-order rate constant to be $k = 3.34\ (0.14) \times 10^{-2}\ (\mathrm{min}^{-1})$.[27] This rate indicates the effectiveness of E2 decomposition using the photocatalyst developed in this study.

We conducted multiple cycles of E2 photodegradation reactions followed by the recovery of CNSnO composite, and confirmed that there is insignificant difference in performance at least during the first three cycles (see Figure S10). It should be noted that while Figure S10 shows the cycling data for CNSnO-0.6, the durability of CNSnO-0.3 is not expected to differ significantly. This suggests that the efficiency of the E2 photodegradation reaction remains consistent over these cycles, highlighting the potential for cyclic utilization of CNSnO composites in the context of such photodegradation reactions.

Finally, we discuss the mechanism by which CNSnO composites contribute to the photodegradation of E2. To understand the mechanism of E2 photodecomposition by

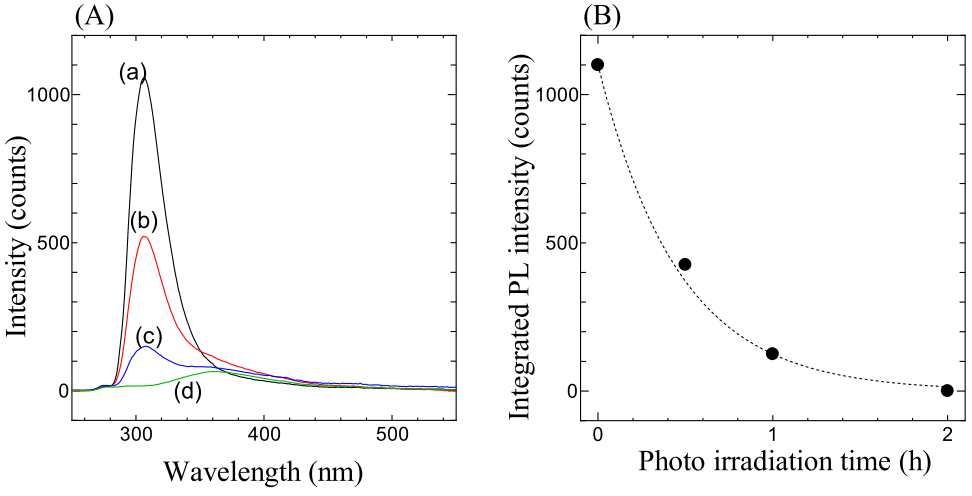

Figure 4. (A) PL intensity of E2 after photoirradiation with CNSnO-0.3 for (a) 0, (b) 0.5, (c) 1.0, and (d) 2.0 h. (B) Integrated PL intensity of E2 as a function of photoirradiation time.

https://doi.org/10.1021/acsomega.4c03390
ACS Omega 2024, 9, 49064−49070

CNSnO-0.3, the surface state of CNSnO-0.3 was examined. The ζ potentials of CNSnO-0 and CNSnO-0.3 in pure water were measured using a Zetasizer Nano ZS (Malvern Panalytical Ltd., UK). The measured ζ potentials were both negative (approximately −35 mV for CNSnO-0 and −55 mV for CNSnO-0.3), indicating that the surface potential of both samples is negative (Table S3). In photocatalytic reactions, it is plausible that the adsorption of the positively polarized parts of water or E2 onto the catalyst surface is the starting point, and this aspect appears to be common to both samples. As previously discussed, the synthesized carbon nitride is structurally similar to g-C_3N_4. However, the band gap of CNSnO-0 (around 2.55 eV), which was evaluated by performing Kubelka−Munk analysis on the observed UV−vis spectrum (Figure S11), is slightly smaller than that of g-C_3N_4 (@2.7 eV).[28] This may be related to the fact that the carbon nitride synthesized in this study is slightly nitrogen-rich, as the band gap of g-C_3N_5 has been reported to decrease to as low as 1.76 eV.[23] Nevertheless, the results confirm that the synthesized carbon nitride is capable of absorbing visible light.

To confirm the bottom energy position of the conduction band in CNSnO-0.3, AC impedance measurements were performed in 1 M KCl aqueous solution, and the complex capacitance was obtained for a Mott−Schottky plot (Figure S12). As shown in Figure S12, the flat-band potential is approximately −1.2 V (vs Ag/AgCl). Since the potential of the Ag/AgCl reference electrode is about +0.2 V relative to the standard hydrogen electrode, it is evident that the conduction band bottom is sufficiently higher than the redox equilibrium potential of oxygen.

Unfortunately, the detailed structure of the Sn oxide contained in the composite is not well understood. However, from XPS, it can be concluded that Sn is in its tetravalent state, suggesting an oxide close to SnO_2.[29] While detailed reports exist on the band gap (approximately 3.65 eV) and band positions of bulk SnO_2, the Sn oxide synthesized in this study consists of amorphous Sn(IV) oxides or ultra fine SnO_2 crystals, which prevents the direct use of the band structure of bulk SnO_2. Furthermore, SnO_2 quantum dots have been reported to have varying band positions and a smaller band gap depending on the synthesis method.[30] However, even with the reduction due to presence of quantum dots, the band gap is unlikely to be smaller than that of carbon nitride. Furthermore, SnO_2 is an n-type semiconductor with its Fermi level near the bottom of the conduction band, while the Fermi level of carbon nitride is near the center of the band gap.[31,32] Therefore, assuming the alignment of the Fermi levels of SnO_2 and carbon nitride results in the schematic band diagram shown in Figure 5. Furthermore, as discussed in the XPS section, the presence of lower-valence tin oxides cannot be ruled out. However, even in that case, the mechanism of E2 photooxidative decomposition by the CNSnO photocatalyst as depicted in Figure 5 is still valid. This is because, although lower-valence tin oxides have a smaller band gap compared to SnO_2, there is not expected to be a significant change in the band alignment with g-CN. In addition to the above, we confirmed through PL measurements whether the separation of excited electron and hole carriers, as shown in Figure 5, is actually occurring in the CNSnO composites (Figure S13). As shown in Figure S13, the PL intensity of CNSnO-0.3 is significantly reduced compared to CNSnO-0. This suggests that the carrier separation, as indicated in Figure 5, is indeed occurring.

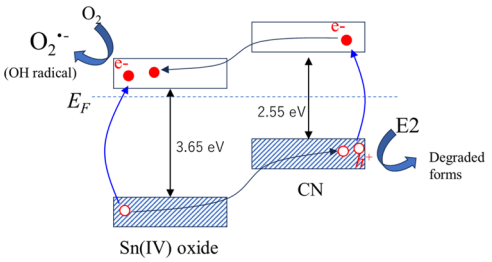

Figure 5. Schematic band diagram of CNSnO composite photocatalyst to explain the photodegradation of E2.

According to the band diagram in Figure 5, we expect that the oxidative decomposition reaction of E2 is induced by holes in the valence band of carbon nitride. On the other hand, reduction reaction should occur to some extent in the conduction band of Sn oxide. To investigate this, ESR experiments were performed using DMPO as a radical trap agent, as described in the experimental section. DMPO can trap both peroxide ion radicals and OH radicals. However, the ESR spectra of DMPO trapped with peroxide ion radicals and DMPO trapped with OH radicals are distinctly different. When comparing the previous research (for example, Figure 9 in ref 33) with Figure 6, it is believed that the radical generated in this experiment is a peroxide ion radical.[33] However, it is also possible that OH radicals are generated via peroxide ions. Therefore, OH radicals are also described in Figure 5. For the E2 photooxidative decomposition by the CNSnO photocatalyst, in addition to the direct oxidation of E2 by holes generated through photoexcitation as depicted in Figure 5, oxidation by OH radicals can also be considered. Ohko et al. have reported that E2 decomposes through DEO via both photooxidation and OH radical oxidation.[25] It is possible that in the CNSnO photocatalyst as well, E2 decomposition proceeds via these two oxidation pathways. The important point is that the reduction reaction of oxygen occurs as the counter-reaction to the E2 photooxidative decomposition. In this experiment, oxygen was not intentionally dissolved in the solution, yet E2 was efficiently photodegraded. This suggests that the photocatalyst developed in this study can be used for

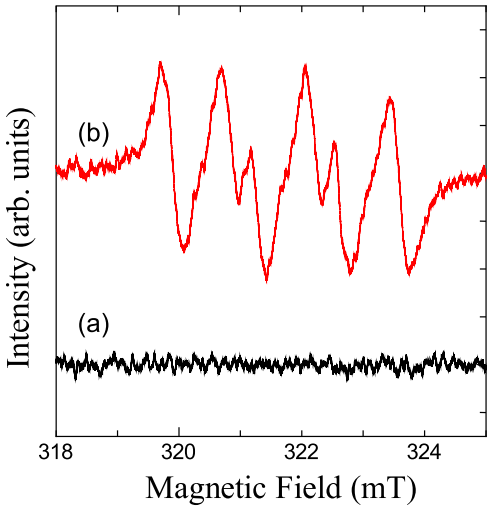

Figure 6. ESR spectra of radical adducts trapped by DMPO (a) before and (b) after photoirradiation.

https://doi.org/10.1021/acsomega.4c03390
ACS Omega 2024, 9, 49064−49070

the photodegradation of estrogen and potentially other endocrine disruptors in river water.

CONCLUSIONS

Several types of composites consisting of tin oxide nanoparticles and graphene-like carbon nitride (g-CN) were synthesized by heating a mixture of urea and tin acetate at 550 °C for 2 h under N_2 flow in an electric furnace. FT-IR measurements revealed that the obtained g-CN possesses structural units similar to g-C_3N_4, a well-studied graphite-like carbon nitride. However, unlike g-C_3N_4, sharp diffraction lines were not observed in the XRD diffraction pattern of g-CN, indicating lower crystallinity. Elemental analysis showed that g-CN is slightly nitrogen-rich compared to g-C_3N_4, and UV−vis measurements indicated that the band gap (2.55 eV) of g-CN is slightly smaller than that of g-C_3N_4 (2.70 eV). When simulated solar light was irradiated on CNSnO-0.3, it efficiently decomposed 17β-estradiol (E2), a natural estrogen. The degradation rate constant was evaluated to be k = 3.34 (0.14) × 10^{-2} (min^{-1}). Peroxide ion radicals were detected in ESR measurements from the irradiated solution, suggesting that peroxide ion radicals are generated through the oxygen photoreduction as the counter-reaction of the oxidative decomposition of E2.

ASSOCIATED CONTENT

Supporting Information

The Supporting Information is available free of charge at https://pubs.acs.org/doi/10.1021/acsomega.4c03390.

Figure S1. Crystal structure of g-C_3N_4, S2. Oxidative degradation process of 17β-estradiol (E2), S3. XRD patterns of (a) CNSnO-0, (b) CNSnO-0.3 and (c) SnO_2 crystal, S4. XRD pattern of g-C_3N_4 prepared from melamine, S5. (A) Sn 3d XPS spectrum of SnO_2 powder sample. (B) C 1s and (C) O 1s XPS spectra of CNSnO-0.3, S6. FE-SEM images of (A) CNSnO-0 and (B) CNSnO-0.3, S7. TEM images of CNSnO-0.3, S8. EDS spectrum of CNSnO-0.3. N, O and Sn mapping images of CNSnO-0.3, S9. The figure with the vertical axis of Figure 4B replotted on a logarithmic scale, S10. Cycling performance of CNSnO-0.6, S11. Tauc plot of CNSnO-0, S12. Mott−Schottky plot of CNSnO-0.3, S13. PL spectra of (a) CNSnO-0 and (b) CNSnO-0.3. Table S1. XPS peak position and peak height of CNSnO-0.3 and SnO_2 powder sample, S2. BET specific surface area of CNSnO samples, S3. ζ Potential of CNSnO-0 and −0.3 (PDF)

AUTHOR INFORMATION

Corresponding Author

Shinji Kawasaki − *Department of Life Science and Applied Chemistry, Nagoya Institute of Technology Gokiso-cho, Nagoya 466-8555, Japan;* orcid.org/0000-0001-8498-987X; Email: kawasaki.shinji@nitech.ac.jp

Authors

Yuzuki Amino − *Department of Life Science and Applied Chemistry, Nagoya Institute of Technology Gokiso-cho, Nagoya 466-8555, Japan*

Ayar Al-zubaidi − *Department of Life Science and Applied Chemistry, Nagoya Institute of Technology Gokiso-cho, Nagoya 466-8555, Japan;* orcid.org/0000-0001-6032-0207

Yosuke Ishii − *Department of Life Science and Applied Chemistry, Nagoya Institute of Technology Gokiso-cho, Nagoya 466-8555, Japan;* orcid.org/0000-0003-0334-2228

Complete contact information is available at: https://pubs.acs.org/10.1021/acsomega.4c03390

Notes

The authors declare no competing financial interest.

ACKNOWLEDGMENTS

This work was financially supported by JSPS KAKENHI grant number 23K23448, by JKA and its promotion funds from KEIRIN RACE.

REFERENCES

(1) Yilmaz, B.; Terekeci, H.; Sandal, S.; Kelestimur, F. Endocrine disrupting chemicals: exposure, effects on human health, mechanism of action, models for testing and strategies for prevention. *Rev. Endocr. Metab. Disord.* **2020**, *21*, 127−147.

(2) Lintelmann, J.; Katayama, A.; Kurihara, N.; Shore, L.; Wenzel, A. Endocrine disruptors in the environment (IUPAC Technical Report). *Pure Appl. Chem.* **2003**, *75*, 631−681.

(3) Peng, Y.; Wang, J.; Wu, C. Determination of Endocrine Disruption Potential of Bisphenol A Alternatives in Food Contact Materials Using In Vitro Assays: State of the Art and Future Challenges. *J. Agric. Food Chem.* **2019**, *67*, 12613−12625.

(4) Phillips, P. J.; Chalmers, A. T.; Gray, J. L.; Kolpin, D. W.; Foreman, W. T.; Wall, G. R. Combined Sewer Overflows: An Environmental Source of Hormones and Wastewater Micropollutants. *Environ. Sci. Technol.* **2012**, *46*, 5336−5343.

(5) Gross-Sorokin, M. Y.; Roast, S. D.; Brighty, G. C. Assessment of Feminization of Male Fish in English Rivers by the Environment Agency of England and Wales. *Environ. Health Perspect.* **2006**, *114*, 147−151.

(6) Luo, J.; Zhang, S.; Sun, M.; Yang, L.; Luo, S.; Crittenden, J. C. A Critical Review on Energy Conversion and Environmental Remediation of Photocatalysts with Remodeling Crystal Lattice, Surface, and Interface. *ACS Nano* **2019**, *13*, 9811−9840.

(7) UshaVipinachandran, V.; Rajendran, S.; Haroon, K. H. B.; Ashokan, I.; Mondal, A.; Bhunia, S. K. Detoxification of Endocrine Disruptors in Water Using Visible-LightActive Nanostructures: A Review. *ACS Appl. Nano Mater.* **2020**, *3*, 11659−11687.

(8) Zhu, Q.; Xu, Z.; Qiu, B.; Xing, M.; Zhang, J. Emerging Cocatalysts on g-C_3N_4 for Photocatalytic Hydrogen Evolution. *Small* **2021**, *17*, No. 2101070.

(9) Yu, X.; Ng, S.; Putri, L. K.; Tan, L.; Mohamed, A. R.; Ong, W. Point-Defect Engineering: Leveraging Imperfections in Graphitic Carbon Nitride (g-C3N4) Photocatalysts toward Artificial Photosynthesis. *Small* **2021**, *17*, No. 2006851.

(10) Xiao, J.; Xie, Y.; Rabeah, J.; Bruckner, A.; Cao, H. Visible-Light Photocatalytic Ozonation Using Graphitic C3N4 Catalysts: A Hydroxyl Radical Manufacturer for Wastewater Treatment. *Acc. Chem. Res.* **2020**, *53*, 1024−1033.

(11) Guan, R.; Li, J.; Zhang, J.; Zhao, Z.; Wang, D.; Zhai, H.; Sun, D. Photocatalytic Performance and Mechanistic Research of ZnO/g-C_3N_4 on Degradation of Methyl Orange. *ACS Omega* **2019**, *4*, 20742−20747.

(12) Gu, Y.; Li, S.; Li, M.; Wang, X.; Liu, Y.; Shi, K.; Bai, X.; Yao, Q.; Wu, Z.; Yao, H. Recent advances in g-C3N4-based photo-enzyme catalysts for degrading organic pollutants. *RSC Adv.* **2023**, *13*, 937−947.

(13) Liu, R.; Chen, Z.; Yao, Y.; Li, Y.; Cheema, W. A.; Wang, D.; Zhu, S. Recent advancements in g-C3N4-based photocatalysts for

photocatalytic CO2 reduction: a mini review. *RSC Adv.* **2020**, *10*, 29408−29418.
(14) Liebig, J. Uber einige stickstoff - verbindungen. *Ann. Pharm.* **1834**, *10*, 1−47.
(15) Wang, X.; Maeda, K.; Thomas, A.; Takanabe, K.; Xin, G.; Carlsson, J. M.; Domen, K.; Antonietti, M. A metal-free polymeric photocatalyst for hydrogen production from water under visible light. *Nat. Mater.* **2009**, *8*, 76−80.
(16) Hassani, A.; Faraji, M.; Eghbali, P. Facile fabrication of mpg-C3N4/Ag/ZnO nanowires/Zn photocatalyst plates for photodegradation of dye pollutant. *J. Photochem. Photobiol., A* **2020**, *400*, No. 112665.
(17) Hassani, A.; Eghbali, P.; Metin, O. Sonocatalytic removal of methylene blue from water solution by cobalt ferrite/mesoporous graphitic carbon nitride (CoFe2O4/mpg-C3N4) nanocomposites: response surface methodology approach. *Environ. Sci. Pollut. Res. Int.* **2018**, *25*, 32140−32155.
(18) Hassani, A.; Krishnan, S.; Scaria, J.; Eghbali, P.; Nidheesh, P. V. Z-scheme photocatalysts for visible-light-driven pollutants degradation: A review on recent advancements. *Curr. Opin. Solid State Mater. Sci.* **2021**, *25*, No. 100941.
(19) Ji, H.; Fan, Y.; Yan, J.; Xu, Y.; She, X.; Gu, J.; Fei, T.; Xu, H.; Li, H. Construction of SnO_2/graphene-like g-C_3N_4 with enhanced visible light photocatalytic activity. *RSC Adv.* **2017**, *7*, 36101−36111.
(20) Putri, L. K.; Ng, B.; Ong, W.; Lee, H. W.; Chang, W. S.; Chai, S. Engineering nanoscale p−n junction via the synergetic dual-doping of p-type boron-doped graphene hybridized with n-type oxygen-doped carbon nitride for enhanced photocatalytic hydrogen evolution. *J. Mater. Chem. A* **2018**, *6*, 3181−3194.
(21) Fina, F.; Callear, S. K.; Carins, G. M.; Irvine, J. T. S. Structural Investigation of Graphitic Carbon Nitride via XRD and Neutron Diffraction. *Chem. Mater.* **2015**, *27*, 2612−2618.
(22) Akgul, F. A.; Gumus, C.; Er, A. O.; Farha, A. H.; Akgul, G.; Ufuktepe, Y.; Liu, Z. Structural and electronic properties of SnO_2. *J. Alloys Compd.* **2013**, *579*, 50−56.
(23) Kumar, P.; Vahidzadeh, E.; Thakur, U. K.; Kar, P.; Alam, K. M.; Goswami, A.; Mahdi, N.; Cui, K.; Bernard, G. M.; Michaelis, V. K.; Shankar, K. C_3N_5: A Low Bandgap Semiconductor Containing an Azo-Linked Carbon Nitride Framework for Photocatalytic, Photovoltaic and Adsorbent Applications. *J. Am. Chem. Soc.* **2019**, *141*, 5415−5436.
(24) Wang, H.; Duan, A.; Mao, J.; Che, B.; Wang, W.; Ma, M.; Wang, Xuedong. Effects of Ionic Liquids on Fluorescence Characteristics of 17α- and 17β-estradiol. *J. Fluoresc.* **2013**, *23*, 103−113.
(25) Ohko, Y.; Iuchi, K.; Niwa, C.; Tatsuma, T.; Nakashima, T.; Iguchi, T.; Kubota, Y.; Fujishima, A. 17β-Estradiol Degradation by TiO_2 Photocatalysis as a Means of Reducing Estrogenic Activity. *Environ. Sci. Technol.* **2002**, *36*, 4175−4181.
(26) Zhao, Y.; Hu, H.; Jin, W. Transformation of Oxidation Products and Reduction of Estrogenic Activity of 17β-Estradiol by a Heterogeneous Photo-Fenton Reaction. *Environ. Sci. Technol.* **2008**, *42*, 5277−5284.
(27) Mitamura, K.; Narukawa, H.; Mizuguchi, T.; Shimada, K. Degradation of estrogen conjugates using titanium dioxide as a photocatalyst. *Anal. Sci.* **2004**, *20*, 3−4.
(28) Zhu, D.; Zhou, Q. Nitrogen doped g-C3N4 with the extremely narrow band gap for excellent photocatalytic activities under visible light. *Appl. Catal., B* **2021**, *281*, No. 119474.
(29) Reddy, C. V.; Babu, B.; Vattikuti, S. V. P.; Ravikumar, R. V. S. S. N.; Shim, J. Structural and optical properties of vanadium doped SnO2 nanoparticles with high photocatalytic activities. *J. Lumin.* **2016**, *179*, 26−34.
(30) Babu, B.; Reddy, I. N.; Yoo, K.; Kim, D.; Shim, J. Bandgap tuning and XPS study of SnO_2 quantum dots. *Mater. Lett.* **2018**, *221*, 211−215.
(31) Villamagua, L.; Stashans, A.; Lee, P.; Liu, Y.; Liu, C.; Carini, M. Change in the electrical conductivity of SnO_2 crystal from n-type to p-type conductivity. *Chem. Phys.* **2015**, *452*, 71−77.
(32) Zhu, B.; Cheng, B.; Zhang, L.; Yu, J. Review on DFT calculation of s-triazine-based carbon nitride. *Carbon Energy* **2019**, *1*, 32−56.
(33) Feng, J.; Jiang, T.; Han, Y.; Okoth, O. K.; Cheng, L.; Zhang, J. Construction of dual Z-scheme Bi_2S_3/Bi_2O_3/WO_3 ternary film with enhanced visible light photoelectrocatalytic performance. *Appl. Surf. Sci.* **2020**, *505*, No. 144632.

https://doi.org/10.1021/acsomega.4c03390
ACS Omega 2024, 9, 49064−49070